Reynolds number and roughness effects on turbulent stresses in sandpaper roughness boundary layers

C. Morrill-Winter, D. T. Squire, J. C. Klewicki, N. Hutchins, M. P. Schultz, and I. Marusic

Phys. Rev. Fluids **2**, 054608 — Published 26 May 2017

DOI: 10.1103/PhysRevFluids.2.054608

Reynolds number and roughness effects on turbulent stresses in sandpaper roughness boundary layers

C. Morrill-Winter, D.T. Squire, N. Hutchins, and I. Marusic
University of Melbourne, Victoria, 3010, Australia[*]

J.C. Klewicki
University of Melbourne, Victoria, 3010, Australia[*] *and*
University of New Hampshire, Durham, NH, 03824, USA.

M.P. Schultz
US Naval Academy, Annapolis, MD 21402-5042, USA
(Dated: May 8, 2017)

Multi-component turbulence measurements in rough-wall boundary layers are presented and compared to smooth-wall data over a large friction Reynolds number range (δ^+). The rough-wall experiments used the same continuous sand-paper sheet as in the study of Squire *et al.* (*J. Fluid Mech.* vol. 795, 2016). To the authors' knowledge, the present measurements are unique in that they cover nearly an order of magnitude in Reynolds number ($\delta^+ \simeq 2,800 - 17,400$) while spanning the transitionally- to fully-rough regimes (equivalent sand-grain-roughness range, $k_s^+ \simeq 37 - 98$), and in doing so also maintain very good spatial resolution. Distinct from previous studies, the inner-normalized wall-normal velocity variances, $\overline{w^2}$, exhibit clear dependencies on both k_s^+ and δ^+ well into the wake region of the boundary layer, and only for fully-rough flows does the outer portion of the profile agree with that in a comparable δ^+ smooth-wall flow. Consistent with the mean dynamical constraints, the inner-normalized Reynolds shear stress profiles in the rough-wall flows are qualitatively similar to their smooth-wall counterparts. Quantitatively, however, at matched Reynolds numbers the peaks in the rough-wall Reynolds shear stress profiles are uniformly located at greater inner-normalized wall-normal positions. The Reynolds stress correlation coefficient, R_{uw}, is also greater in rough-wall flows at a matched Reynolds number. As in smooth-wall flows, R_{uw} decreases with Reynolds number, but at different rates depending on the roughness condition. Despite the clear variations in the R_{uw} profiles with roughness, inertial layer u, w cospectra evidence invariance with k_s^+ when normalized with the distance from the wall. Comparison of the normalized contributions to the Reynolds stress from the second quadrant (Q2) and fourth quadrant (Q4) exhibit noticeable differences between the smooth- and rough-wall flows. The overall time fraction spent in each quadrant is, however, shown to be nearly fixed for all of the flow conditions investigated. The data indicate that at fixed δ^+ both Q2 and Q4 events exhibit a sensitivity to k_s^+. The present results are discussed relative to the combined influences of roughness and Reynolds number on the scaling behaviours of boundary layers.

I. INTRODUCTION

Turbulent boundary layers over rough-walls are of considerable practical interest, since, for example, most applications involve surfaces that are, or become over time, dynamically rough. More generally, the study of rough-wall turbulence holds potential to provide new insights regarding the possible effects of the wall boundary condition on wall-turbulence structure. Inquiries into these effects are relevant to the dynamics underlying all turbulent wall-flows, and especially in connection with modifying the mechanisms of wall-normal momentum and scalar transport.

The direct practical importance of high quality rough-wall turbulence measurements, and the broader issue of flow sensitivities to the wall boundary condition, motivate the present study of turbulent stress behaviours in boundary layer flows over smooth- and rough-walls over comparable Reynolds number ranges. The remainder of this Introduction articulates the primary issues to be investigated. Throughout, variants of u, v and w are used to denote the velocity components in the streamwise (x), spanwise (y) and wall-normal (z) directions, with upper case symbols denoting mean quantities and an overbar indicating the application of the time average. Also, a superscript + denotes normalisation by inner variables: lengths normalised by ν/U_τ and velocities normalised by U_τ, where ν is the kinematic viscosity, and U_τ is the friction velocity.

* squired@unimelb.edu.au

Surface roughness effects on the mean streamwise velocity profile have been extensively studied, and these effects are generally well-accepted, e.g. [1]. Clauser [2] and Hama [3] (and many researchers since) showed that the streamwise mean velocity profile over a rough-wall exhibits a region of log-linear dependence, as it does in smooth-wall flows. This region is, however, shifted downward on the profile graph relative to the smooth-wall profile by an amount, ΔU^+, that is commonly called the roughness function. Physically, the shift indicated by the roughness function is due to the increased drag of the rough surface. Thus, the mean velocity profile in the logarithmic region of a rough-wall flow can be expressed as

$$U^+ = \frac{1}{\kappa}\log(z+\epsilon)^+ + A - \Delta U^+, \tag{1}$$

where κ and A are the smooth-wall log-law constants and ϵ, the zero-plane displacement, accounts for the roughness itself displacing the entire flow away from the wall. In contrast to current understanding of roughness effects on the mean flow, there is significant uncertainty regarding how rough surfaces affect turbulence quantities, modify transport mechanisms, or influence the overall structure of the boundary layer. Accordingly, this study complements the recently published investigation of Squire *et al.* [4], which documented the properties of the mean velocity, U, and streamwise turbulent stress, $\overline{u^2}$, over a similar range of Reynolds numbers and roughness conditions.

The 'k-type' roughness is most associated with flows of practical interest [5]. These include homogeneously distributed roughness of the kind whose effects are studied herein. Within the k-type classification, one can further organize flow behaviours within two regimes that are distinct from smooth-wall flows. These regimes depend on the magnitude of ΔU^+ [6]. At finite but sufficiently small ΔU^+ ($\lesssim 7$), the net drag of the surface derives from a complex mixture of both viscous and pressure effects acting directly on the roughness elements. The flow in this roughness regime is termed *transitionally rough*. At larger ΔU^+ fully rough flows are observed, whereby the pressure drag associated with flow separation from the roughness elements dominates the contribution to the overall drag. The fully rough condition is defined by a ΔU^+ that is a log-linear function of k^+, where k is a representation of the roughness height. It is important, however, to note that the fully rough condition does not necessarily imply that the mean dynamics above the roughness elements are devoid of a leading order viscous effect [4, 7, 8].

In rough-wall flow studies it is pragmatic, and thus common practice, to employ Nikuradse's [9] equivalent sandgrain roughness, k_s. This practice forces all fully-rough flows to adhere to the log-linear fully-rough asymptote

$$\Delta U^+ = \frac{1}{\kappa}\log k_s^+ + A - A'_{FR}. \tag{2}$$

The constant $A'_{FR} = 8.5$ was empirically determined by Nikuradse [9] using a variety of sand grain roughness surfaces. With this definition, k_s^+, like ΔU^+, provides a representation of the rough-wall drag increment relative to the smooth-wall, permitting comparisons between flows above geometrically different roughnesses.

A large number of rough-wall studies in the existing literature investigate the validity of Townsend's wall similarity hypothesis [10]. Here it is hypothesized that at sufficiently high Reynolds number there is an outer flow region where statistical profiles are unaffected by viscosity, except through the boundary conditions which set the velocity scale, U_τ, and the boundary layer thickness length scale, δ [1]. Townsend's hypothesis remains a subject of ongoing investigation, with numerous studies suggesting its validity [e.g., 11–16], and a smaller but significant number indicating violations of the hypothesis [e.g., 17–22]. Ramifications associated with the validity of Townsend's hypothesis pertain to the degree that roughness perturbations remain embedded within the turbulence structure, or more broadly, influence the underlying dynamics. By itself, however, the hypothesis is somewhat ambiguous relative to addressing these questions, since it speaks fundamentally to statistical measures, and not necessarily to the instantaneous motions that contribute to these measures. These considerations motivate aspects of the present study to better understand under what conditions and why Townsend's hypothesis is apparently satisfied.

The predominant empirical test for wall-similarity is to inner-normalise a given velocity statistic, and then compare smooth- and rough-wall profiles with $(z+\epsilon)/\delta$ on the abscissa. Such comparisons are influenced by errors in U_τ and z, both of which can be difficult to estimate in rough-wall flows. It is additionally important to keep in mind that the wall similarity hypothesis is based on an asymptotic (high Reynolds number) approximation, and pertains to a region beyond where wall perturbations directly affect the flow. Assessing wall similarity is thus further complicated in experiments where δ^+ is low, the roughness geometry generates motions of $\mathcal{O}(\delta)$ size, or both. Jiménez [6] analyzed data from a range of extant rough-wall studies, and from this suggested that for wall similarity to be operative, δ/k must be larger than approximately 40. There are, however, studies that do not observe wall similarity, even though they satisfy this approximate threshold, e.g. [23]. Jimenez [6] cites a need for measurements in which δ/k and k^+ are both large (low blockage, fully-rough flow), and where δ/k is large and k^+ is small (low blockage, transitionally-rough flow), to help clarify ongoing questions regarding the physics of rough-wall flows. In terms of how the roughness induced motions *assimilate* within the turbulence, such considerations are consistent with recent findings indicating

that the combined roughness and Reynolds number problem is of a richer complexity than can be adequately captured within the transitionally-rough and fully-rough characterizations alone [4, 7, 8, 24].

The present investigation complements the recent studies by Squire *et al.* [4, 25, 26], which analyzed well-resolved streamwise velocity measurements over an unprecedented range of k_s^+ and δ^+, and included u data acquired using the multi-element hot-wire sensor of Morrill-Winter *et al.* [27]. In particular, we here extend the rough-wall study of Squire *et al.* [4] by analyzing the wall-normal velocity and Reynolds shear stress measurements. This includes comparisons with the smooth-wall measurements of Morrill-Winter *et al.* [27], also acquired with the same sensor and over a comparable Reynolds number range. To the authors' knowledge, the present measurements are unique in that they cover nearly an order of magnitude in Reynolds number ($\delta^+ \simeq 2,800 - 17,400$) while spanning the transitionally- to fully-rough regimes (equivalent sand-grain-roughness range, $k_s^+ \simeq 37 - 98$), and in doing so also maintain very good spatial resolution. Per the above discussion, the present aims include documenting and further clarifying how the combined influences of roughness and Reynolds number conspire to produce the net momentum transport and observed statistical features of the flow. Throughout the remainder of this paper, x, y and z denote the streamwise, spanwise and wall-normal directions, respectively, with $z = 0$ located at the roughness crest.

II. EXPERIMENTAL DETAILS

The rough-wall measurements were acquired in the flow above P36 grit sandpaper in the High Reynolds Number Boundary Layer Wind Tunnel (HRNBLWT), e.g. [28, 29]. These experiments are described in Squire *et al.* [4], and thus only details specific to the present paper are summarised here. The sandpaper roughness elevation, h, is normally distributed, with $k = 6\sigma(h) = 0.902$ mm and $k_s = 1.96$ mm. Multi-wire hotwire sensor measurements were acquired at three different streamwise locations ($x \approx 7$ m, 15 m and 21.7 m), and at three freestream velocities ($U_\infty \approx 7$ m/s, 12 m/s and 17 m/s). The resulting nine experiments span the range of roughness parameters shown in Fig. 1, and over the friction Reynolds number range $2800 < \delta^+ < 17400$. The smooth-wall measurements were obtained in the HRNBLWT and in the Flow Physics Facility (FPF) at the University of New Hampshire, and span the Reynolds number range $2600 < \delta^+ < 12500$ [27]. Table I presents properties of the rough-wall boundary layers studied herein. It is noted that here δ is defined as the wall-normal location at which the mean streamwise velocity is 99% of the freestream velocity, U_∞.

The multi-element hot-wire probe employed is similar to that used by Foss and Haw [30], but is considerably smaller. The probe, which consists of a vertical $\times$-array and two wall-parallel single wires (all wires have equal length l), is contained within a volume of $\Delta x \times \Delta y \times \Delta z = 0.4$ mm $\times$ 0.4 mm $\times$ 0.5 mm. None of these dimensions exceed 25 wall units across all smooth- and rough-wall measurements (see table I). As described in Morrill-Winter *et al.* [27], under the current processing the sensor yields measurements of $\tilde{u}$, w, uw and $\tilde{\omega}_y$. Here $\tilde{\cdot}$ represents a total quantity (mean plus fluctuation), and ω_y is the spanwise vorticity. (Note that in Morrill-Winter *et al.* [27] the sensor is referred to as the ω_z probe because they employed y as the wall-normal coordinate.) One novel aspect of the sensor is that the parallel- and cross-wire- arrays are interwoven to symmetrically center the effective measurement point. A second is its unique calibration and processing scheme that solves for w absent its mean value, while independently determining $\tilde{u}$ from the single wires [27]. This, for example, results in a greater level of consistency in the Reynolds stress profiles.

The friction velocity, U_τ, is determined for the rough-wall data using the approach described in Squire *et al.* [4]. This approach uses the large floating element drag balance that is located in the Melbourne Wind Tunnel between $x = 19.5$ m and $x = 22.5$ m downstream of the beginning of the test section. Baars *et al.* [31] used this drag balance to determine the mean wall-drag on the rough-wall at $x = 21$ m across a wide range of freestream velocities. For rough-wall profiles obtained above the drag balance (i.e., profiles acquired at $x = 21.7$ m) the drag balance readings can be used to determine U_τ directly with a maximum error at $U_\infty \approx 5$ m/s of 2.5% [4, 31]. The error is less when U_∞ is larger. For the profiles not acquired above the drag balance, we employ a novel form of the modified Clauser method. In this approach, the data taken above the drag balance are used to determine the characteristic relationship between roughness function, ΔU^+, and equivalent sandgrain roughness, k_s^+, and this relationship is assumed to be universal for a particular roughness. In this manner, the data obtained above the drag balance yield $\Delta U^+ = f(U_\tau, \nu)$, thus eliminating one fitted parameter from the conventional modified Clauser approach. Fig. 1(b) shows the roughness function relationship, determined directly using the drag balance measurements of Baars *et al.* [31]. The black line shows a smoothing spline fit to a cubic interpolation of the data taken above the drag balance. We determine U_τ at $x \not\approx 21$ m by forcing conformity to the fitted curve, and by minimizing the least-squares error between the inner-normalised streamwise velocity profile and the rough-wall logarithmic law (equation 1). Here we use $\kappa = 0.39$ and $A = 4.3$ given by Marusic *et al.* [32], with justification provided in Squire *et al.* [4].

The approach described above requires a knowledge of both the zero-plane displacement, ϵ, and the region over which the logarithmic law should apply (commonly called the inertial sublayer). We assume $\epsilon = k/2$, but note that any sensible choice of ϵ ($0 < \epsilon < k$) does not appreciably change the results presented herein [4]. To estimate the

TABLE I. Properties of the rough-wall boundary layers studied herein, as acquired in the HRNBLWT at the University of Melbourne. Also included are the sensor wire length, l^+, and wire spacing, Δy^+. The boundary layer thickness, δ, is defined as the wall-normal location at which the mean streamwise velocity is 99% of the freestream velocity, U_∞. Note that *transitionally rough* flows are characterized by $k_s^+ \lesssim 70$, while *fully rough* flows are characterized by $k_s^+ \gtrsim 70$.

symbol	δ^+	k_s^+	z_I^+	U_∞ (m/s)	ΔU^+	u_τ (m/s)	ν/u_τ $(10^{-6}\,m)$	l^+ Δz^+	Δy^+
■	2890	41	365	7.3	4.5	0.314	48.2	10.4	8.5
◆	5190	38	531	7.2	4.2	0.290	51.5	9.7	8.0
■	5250	68	535	12.1	6.3	0.529	28.5	17.5	14.4
●	6770	37	629	7.3	4.2	0.287	52.4	9.5	7.8
■	7670	97	682	17.1	7.4	0.754	20.1	24.9	20.4
◆	8980	66	754	12.2	6.1	0.503	29.6	16.9	13.9
●	12300	63	922	12.2	6.0	0.488	31.1	16.1	13.2
◆	13140	93	962	17.4	7.2	0.718	21.1	23.7	19.4
●	17190	89	1143	17.3	7.1	0.698	21.9	22.9	18.8

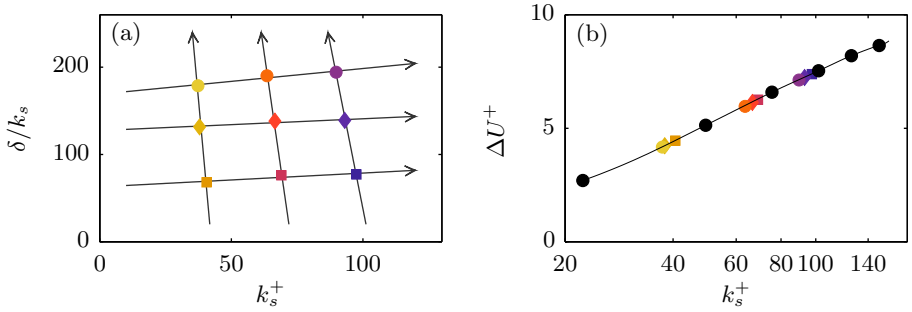

FIG. 1. Visual representation of tabulated parameters. (a) inner-normalized roughness height versus boundary-layer-roughness-height scale separation. (b) roughness function as a function of inner normalized roughness height. Black circles are the profiles coupled with the drag balance; the black line is a smoothing spline fit to a cubic interpolation of the black circles.

wall-normal location of the start of the logarithmic region, we follow the work of Mehdi *et al.* [7]. Guided by the mean momentum balance, they showed convincing evidence that the location of the inertial layer for rough walls does not scale on k or δ as classically assumed, but instead scales with the location of the peak in the Reynolds shear stress. These authors developed empirical expressions for this location, z_m, that depend on the three length scales present in rough-wall flows (ν/U_τ, k and δ), and suggest that for $z_m/k_s > \mathcal{O}(1)$, which encompasses all data presented herein, the onset of the inertial sublayer, z_I, can be approximated as:

$$\begin{aligned} z_I &= C_I \times z_m \\ &= C_I \times 0.89(\nu/U_\tau)^{0.36} k_s^0 \delta^{0.64} \end{aligned} \tag{3}$$

Note that here z_I physically denotes the smallest wall-normal location at which, to leading order, the mean dynamics are wholly inertial. Equation 3 is, however, appropriate only for rough wall flows with $z_m/k_s > \mathcal{O}(1)$. The flow above the present rough surface has been shown to exhibit a logarithmic region, in both the mean and streamwise velocity variance, that spans $z_I < z + \epsilon < 0.19\delta$, where z_I is determined from equation 3 with $C_I = 2.5$ [4]. Hence, these bounds are also employed in the present study. For the smooth-wall data, U_τ is determined using the composite fit of Chauhan *et al.* [33] across an inertial sublayer spanning $z_I = 3\sqrt{\delta\nu/U_\tau} < z + \epsilon < 0.19\delta$, with $\kappa = 0.39$ and $A = 4.3$ [4, 32].

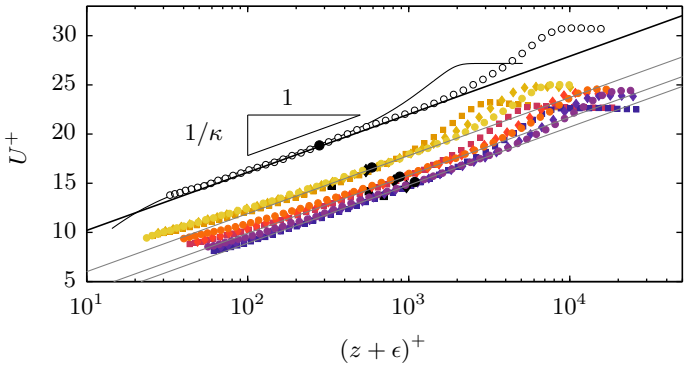

FIG. 2. Mean velocity profiles normalized by inner variable. The solid black line is $U^+ = 0.39^{-1}\log(z^+ + \epsilon^+) + 4.3$ ([32]). Symbols are given in table I. The black comparison profile is from the DNS of Sillero et al. [34] at $\delta^+ \simeq 2000$, and ○ is the $\delta^+ \simeq 7900$ smooth wall data presented in Morrill-Winter et al. [27]. The large black symbols show the onset of inertial dynamics, z_I, for each profile according to the formulation of Mehdi et al. [7]. Note that transitionally rough flows are characterized by $k_s^+ \lesssim 70$, while fully rough flows are characterized by $k_s^+ \gtrsim 70$.

III. RESULTS

Figure 2 presents inner-normalized mean velocity profiles over the rough walls. Taking into account that the onset of the inertial domain here is demarcated by z_I and not the classically assumed roughness crest, the profiles show a convincing logarithmic dependence that is well described by $\kappa = 0.39$. The expected downward shifts, ΔU^+, are apparent. As clearly depicted in Fig. 1a, the parameter space of these experiments is given by three k_s^+ values (at $k_s/\delta \simeq$ const.), and three k_s/δ values (at $k_s^+ \simeq$ const.). Comparisons are made with smooth-wall boundary layers from the DNS of Sillero *et al.* [34] at $\delta^+ \simeq 2,000$, and from the Melbourne Wind Tunnel at $\delta^+ \simeq 7,900$ [27]. The profiles of $\Delta U^+ \simeq 4.2$ and $\Delta U^+ \simeq 6.2$ exhibit a greater near wall deviation from the log-law than the $\Delta U^+ \simeq 7.2$ case. Although no conclusion is drawn here, the consistency of the trend points to the process by which the near wall dynamics change with increasing k_s^+ through the transitionally-rough to fully-rough regime. More details on the mean velocity profiles for this experimental campaign are given in Squire *et al.* [4].

A. Turbulent stresses

Statistical profiles associated with the fluctuations of velocity components are often presented under an inner-outer normalization to deduce whether the results are in support of Townsend's similarity hypothesis [e.g., 35]. The present $\overline{uw}^+$, $\overline{w^2}^+$ and $\overline{u^2}^+$ profiles are plotted in Figs. 3, 4 and 5, respectively. Note that the $\overline{u^2}^+$ profiles were previously discussed and analysed by Squire *et al.* [4], but are reproduced here for completeness. Figs. 3, 4 and 5 are not plotted on a linear abscissa, as doing so tends to imply that the domain of similarity begins at a fixed $(z+\epsilon)/\delta$ location. Consistent with previous studies [4, 7, 8], the outer similarity argument is considered herein relative to a domain starting near z_I – a position that generally moves to smaller $(z+\epsilon)/\delta$ with increasing δ^+.

Although the rough-wall Reynolds shear stress profiles of Fig. 3a have shapes similar to those found in smooth-wall flows, relative to inner-normalized wall position, they exhibit a less rapid near-wall increase. The rough-wall data do, however, monotonically increase to peak at an intermediate wall location (as in smooth-wall flows), and beyond this position they monotonically decrease to zero to satisfy the outer boundary condition. Note, that the peak in $-\overline{uw}^+$ occurs at the location, z_m, where the Reynolds stress gradient crosses zero. This position can be thought of as a surrogate for where the turbulent inertia transitions from a momentum source to sink [7, 36]. The peak magnitudes of $-\overline{uw}^+$ are in agreement with $-\overline{uw}^+ \to 1$ as $\delta^+ \to \infty$, e.g., [37]. The viscous stress becomes negligible at a small distance from the wall, and as δ^+ increases, $\mathcal{O}(z_m) \gg \mathcal{O}(\nu/U_\tau)$. This coincides with the formation of a diminishing curvature plateau in the profile over which $-\overline{uw} \simeq U_\tau^2$. Squire *et al.* [4] show that the present data adhere to this relationship to within ±2%, thus evidencing a high level of agreement between the present method of estimating the mean wall shear stress, and the peak magnitude of the Reynolds stress.

Prevalent descriptions presume that in fully rough flows the maximum of $-\overline{uw}^+$ is located near the crest plane of the roughness. This implies that the totality of the positive Reynolds stress gradient resides within the roughness canopy, regardless of δ^+. The total integral of $\partial\overline{uw}^+/\partial z^+$ is zero in both smooth- and rough-wall flows, and thus the

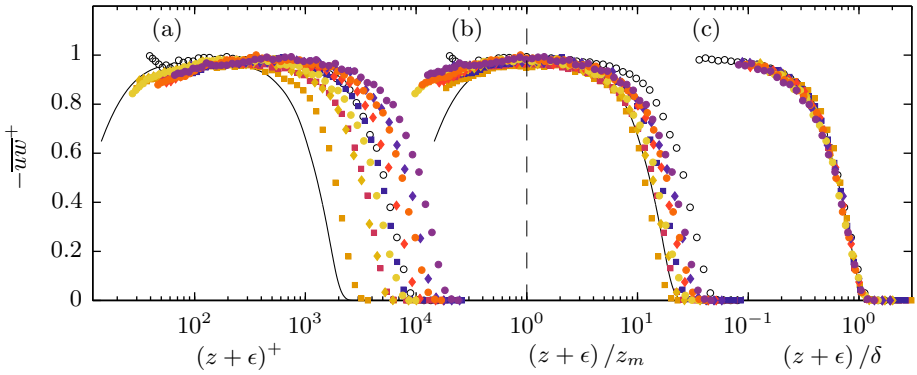

FIG. 3. Inner-normalized Reynolds stress profile plotted with respect to inner (a), intermediate (b) outer normalized (c) wall position above the rough-wall. The dashed line in (b) shows $(z+\epsilon)/z_m = 1$. The profiles in (c) are only plotted for $(z+\epsilon)/\delta > z_I/\delta$. Recall $z_I = 2.5 \times z_m$. Symbols are given in table I. The black comparison profile is the DNS of Sillero *et al.* [34] at $\delta^+ \simeq 2000$, and ○ is the $\delta^+ \simeq 7900$ smooth wall data presented in Morrill-Winter *et al.* [27].

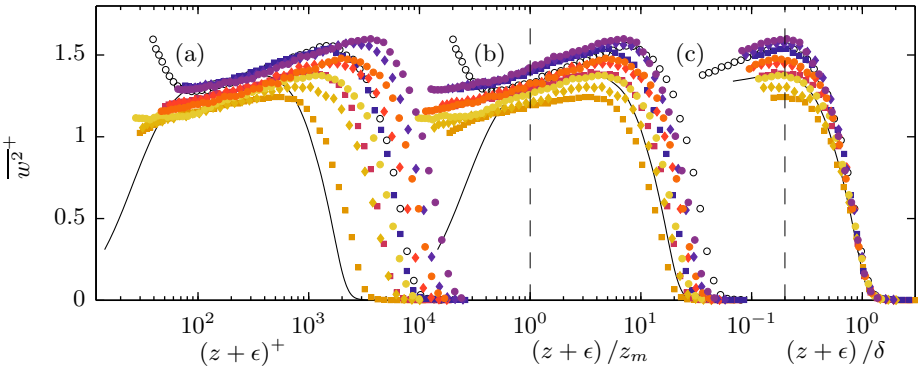

FIG. 4. Inner-normalized wall-normal velocity variance plotted with respect to inner (a), intermediate (b) outer normalized (c) wall position above the rough-wall. The dashed lines in (b) and (c) show $(z+\epsilon)/z_m = 1$ and $(z+\epsilon)/\delta = 0.2$, respectively. The profiles in (c) are only plotted for $(z+\epsilon)/\delta > z_I/\delta$. Recall $z_I = 2.5 \times z_m$. Symbols are given in table I. The black comparison profile is from the DNS of Sillero *et al.* [34] at $\delta^+ \simeq 2000$, and ○ is the $\delta^+ \simeq 7894$ smooth wall data presented in Morrill-Winter *et al.* [27].

positive contribution to the Reynolds stress gradient always balances the negative portion [7]. The consequences of this are worth exploring in greater depth, especially since Squire *et al.* [4] provide clear evidence that the onset of the log-region for both the mean and streamwise variance is closely approximated by equation 3 (recall $z_I = C_I \times z_m$, where z_m is the wall-normal location of the peak in the Reynolds shear stress). The precise peak location of $-\overline{uw}^+$ is challenging to determine with experimental data, and especially as δ^+ increases. This is because the curvature of the Reynolds stress profile, $\partial^2\left(-\overline{uw}^+\right)/\partial z^{+2}$, diminishes with increasing δ^+. Given this, z_m was estimated using Eq. 3, and Fig. 3b plots $-\overline{uw}^+$ versus $(z+\epsilon)/z_m$. It is apparent that the $(z+\epsilon)/z_m$ coordinate approximately aligns the maxima in $-\overline{uw}^+$. Admittedly, however, the noted limitations of experimental accuracy only allow a qualitative assessment.

Figure 3c plots $-\overline{uw}^+$ for $z+\epsilon \geq z_I$ against outer normalized wall height. These data convincingly support an invariant $-\overline{uw}^+$ profile on an inertial outer domain (of width that approaches δ as $\delta^+ \to \infty$) that is specified through consideration of the leading order balances in the mean momentum equation. As $\delta^+ \to \infty$, this curve will continue to extend towards zero while increasing in magnitude to unity. These behaviours are consistent with the classical notion of outer layer similarity, but here the relevant domain is more precisely specified within the context of properties exhibited by the mean dynamical equation. The net force developed by the Reynolds stress is $\partial(-\rho\overline{uw})/\partial z$. Therefore, the merging of the Reynolds shear stress profiles observed beyond z_I (Fig. 3c) indicates a loss of sensitivity to roughness and Reynolds number. This finding is in line with the similarity that is observed in the mean velocity profiles in defect form [4].

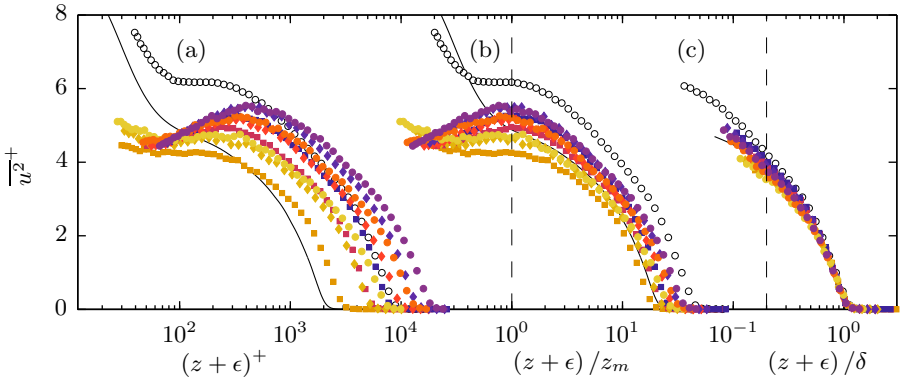

FIG. 5. Inner-normalized streamwise velocity variance plotted with respect to inner (a), intermediate (b), outer normalized (c) wall position above the rough-wall. The dashed lines in (b) and (c) show $(z+\epsilon)/z_m = 1$ and $(z+\epsilon)/\delta = 0.2$, respectively. The profiles in (c) are only plotted for $(z+\epsilon)/\delta > z_I/\delta$. Recall $z_I = 2.5 \times z_m$. Symbols are given in table I. The black comparison profile is from the DNS of Sillero *et al.* [34] at $\delta^+ \simeq 2000$, and ○ is the $\delta^+ \simeq 7894$ smooth wall data presented in Morrill-Winter *et al.* [27].

The wall-normal variance profiles of Fig. 4 exhibit more complicated dependencies on k_s^+ and δ^+ than the Reynolds stress profiles, and share some similarities in trend with the streamwise velocity variance profiles reported in Squire *et al.* [4], also see Fig. 9. For the parameter ranges considered, a clear k_s^+ effect is observed in the outer portion of the flow. Although the present experiments do not explicitly segregate roughness and friction Reynolds number effects, it is evident that as the flow approaches the fully rough regime the agreement between the smooth- and rough-wall profiles improves. Morrill-Winter *et al.* [27] found that for smooth-wall flows over $2000 \lesssim \delta^+ \lesssim 12,500$ the $\overline{w^2}^+$ profiles merge near $(z+\epsilon)^+ = 80$, and for greater $(z+\epsilon)^+$ follow a similar upward trajectory until $(z+\epsilon)/\delta \simeq 0.2$. Here the profiles attain their peak magnitude, and for greater $(z+\epsilon)/\delta$ subsequently decrease to satisfy the outer boundary condition. (Note that hereafter $\overline{w^2}^+_{80}$ refers to $\overline{w^2}^+$ evaluated at $(z+\epsilon)^+ = 80$.) The rough-wall profiles exhibit similar behaviours. For $k_s^+ \lesssim 80$, however, these profiles exhibit a relative downward shift over the domain $(z+\epsilon)^+ \geq 80$. These data also suggest a near wall k_s^+ influence on $\overline{w^2}^+$, while the observed relative magnitude increase with increasing $(z+\epsilon)^+$ is apparently preserved. That is, the rate of increase from $(z+\epsilon)^+ \simeq 80$ to $(z+\epsilon)/\delta \simeq 0.2$ remains essentially unchanged. Here we also note that the downward shift in magnitude is not thought to be a normalization issue (i.e., not a U_τ issue), since the Reynolds stress profiles exhibit a high level of consistency, also see [4].

Figure 4c plots $\overline{w^2}^+$ under outer-normalization by, once again, only including positions $(z+\epsilon) \geq z_I$. This representation reinforces the previous observation that the peaks of the $\overline{w^2}^+$ profiles align at $(z+\epsilon)/\delta \simeq 0.2$. Clearly there is no outer layer similarity for the parameter ranges considered here. This observation, however, does not necessarily disagree with the classical argument. Namely, outer layer similarity may require much higher Reynolds numbers before the $\overline{w^2}^+$ profile begins to approximate its limiting value. For example, Kunkel and Marusic [38] present $\overline{w^2}^+$ data for a large range of δ^+, including from the atmospheric surface layer. These authors developed a formulation, guided by their data, that approximates the asymptotic behaviour of $\overline{w^2}^+$. With the criteria used herein and by Squire *et al.* [4] to detect evidence of outer layer similarity, their formulation predicts that similarity is satisfied in smooth-wall flows (to within a small uncertainty) for $\delta^+ > 10^5$. Squire *et al.* [4] show that the k_s^+ effect on outer layer similarity for $\overline{u^2}^+$ is only a weak function of δ^+. With this, it seems likely that for the present roughness there is a minimum $\delta^+(k_s^+)$ threshold at which outer similarity in $\overline{w^2}^+$ is approximated.

To explore this further, Fig. 6 plots the maximum values in $\overline{w^2}^+$ versus friction Reynolds number. For reference, the peak growth function of Kunkel and Marusic [38] is included along with all the smooth wall data of Morrill-Winter *et al.* [27], and the highest δ^+ data from the DNS of Sillero *et al.* [34]. The horizontal black dashed line is the asymptotic limit given by Kunkel and Marusic [38] based on Townsend's [10] attached eddy hypothesis. As is evident, the fully-rough data in Fig. 6 trend with δ^+ in a manner similar to the smooth wall case. For the transitionally rough data the growth rate with increasing δ^+ does, however, seem to be slightly larger. This behaviour is highlighted by the logarithmic line fitted through the constant k_s^+ data points (given as the black lines in Fig. 6). Here it is apparent that the growth rate becomes a decreasing function of k_s^+. It is not possible with the present data to determine conclusively

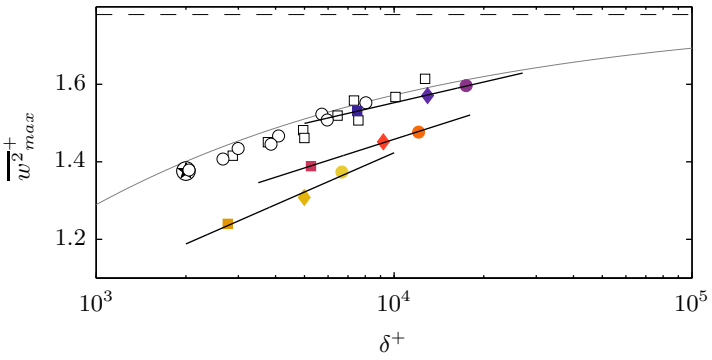

FIG. 6. The peak magnitude of $\overline{w^2}^+$ with increasing δ^+. The rough wall symbols are tabulated in I. The open symbols are the smooth-wall data of Morrill-Winter *et al.* [27] (refer to publication for boundary layer parameters): ○ represent data acquired in the Melbourne Wind Tunnel, where □ signify data taken in the FPF. The ⊛ comparison point is from the Sillero *et al.* [34] DNS at $\delta^+ \simeq 2000$. The gray line is the peak function from Kunkel and Marusic [38] and the horizontal black dashed line is the asymptotic limit they gave of 1.78. The black lines represent the least square logarithmic fit for each of the k_s^+ groupings. These fit lines should be simply considered a visual aid since we have no theoretical reason to suppose that a logarithmic function is the appropriate form for the peak growth.

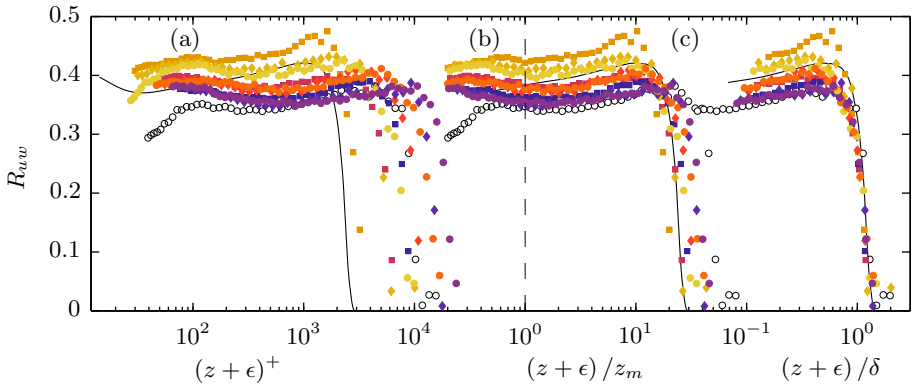

FIG. 7. Inner-normalized Reynolds stress correlation coefficient profile plotted with respect to inner (a), intermediate (b) outer normalized (c) wall position above the rough-wall. The profiles in (c) are only plotted for $(z+\epsilon)/\delta > z_I/\delta$. Recall $z_I = 2.5 \times z_m$. Symbols are given in table I. The black comparison profile is from the DNS of Sillero *et al.* [34] at $\delta^+ \simeq 2000$, and ○ is the $\delta^+ \simeq 7894$ smooth wall data presented in Morrill-Winter *et al.* [27].

whether the dependency of $\overline{w^2}^+_{max}$ on k_s^+ is lost at sufficiently high δ^+, though the results of Fig. 6 provide ostensible evidence that this is indeed the case (certainly, such behaviour is observed for $\overline{u^2}^+$ in the outer region – see Squire *et al.* [4]). This apparent behaviour is consistent with Townsend's [10] wall-similarity and attached eddy hypotheses.

B. Unravelling roughness and Reynolds number effects

Reynolds shear stress implies the non-zero correlation of u and w. However, both the $\overline{u^2}^+$ profiles of Squire *et al.* [4] and the present $\overline{w^2}^+$ profiles exhibit significant dependencies on k_s^+ and δ^+. The trends indicative of these behaviours are captured in Fig. 4 above and Fig. 9 below. These trends are dramatic relative to the more subtle variations exhibited by the $\overline{uw}^+$ profiles of Fig. 3. Collectively, these observations indicate that the wallward turbulent momentum flux in these flows varies considerably relative to the intensities of u and w, and this is reflected in the Reynolds stress correlation coefficient ($R_{uw} = -\overline{uw}/(\sqrt{\overline{u^2}}\sqrt{\overline{w^2}})$) profiles shown in Fig. 7. Qualitatively, these profiles reveal the existence of a clear Reynolds number dependence, and that surface roughness modifies this dependence. Of particular note is the $(z+\epsilon)/z_m$ normalization (Fig. 7), which shows that the onset of the inertial domain appears to

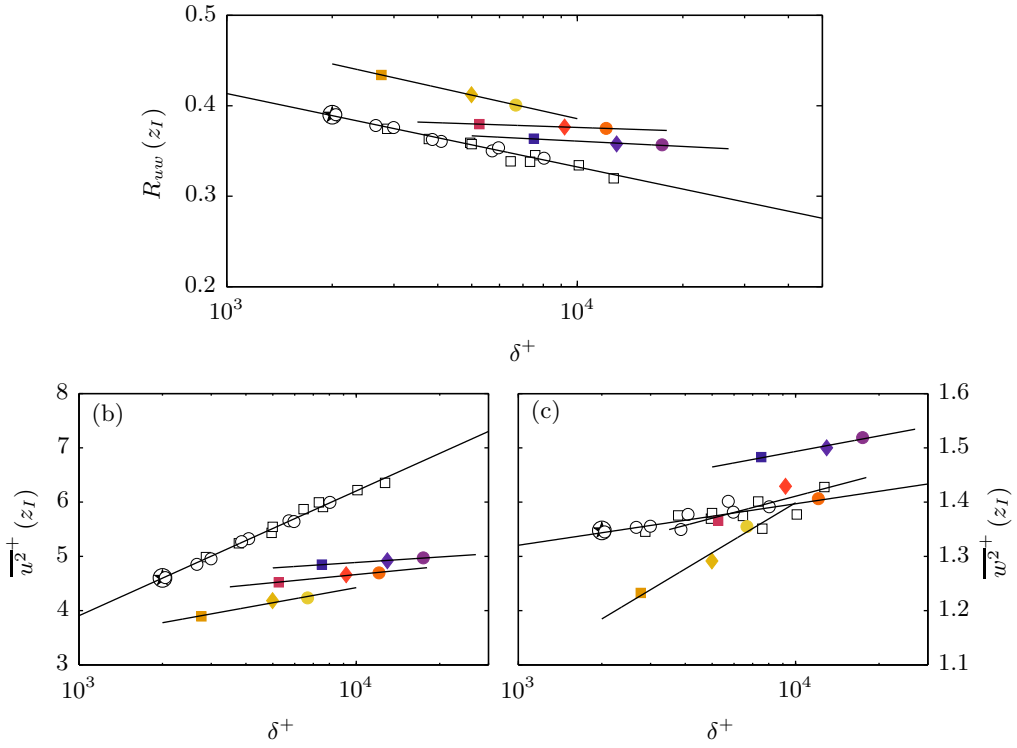

FIG. 8. Reynolds stress correlation coefficient (a), streamwise velocity variance (b), and wall-normal velocity variance (c) at the onset of the inertial domain plotted with respect to δ^+. The rough wall symbols are tabulated in I. The open symbols are all the smooth-wall data of Morrill-Winter *et al.* [27] (refer to publication for boundary layer parameters): ○ represent data acquired in the Melbourne Wind Tunnel, where □ signify data taken in the FPF. The ⊛ comparison point is from the Sillero *et al.* [34] DNS at $\delta^+ \simeq 2000$. The black lines represent the least square logarithmic fit for each of the k_s^+ groupings.

nominally coincide with a local minimum in the R_{uw} profile. (Recall here that $z_I = C_I z_m$.) Accordingly, under inner and outer normalization, z_I respectively moves to increasing $(z+\epsilon)^+$ and decreasing $(z+\epsilon)/\delta$ with increasing δ^+.

A better understanding of the flow behaviours underlying the profiles of Fig. 3 is gained by clarifying the relative effects of roughness and Reynolds number on the turbulence mechanism for wall-normal momentum transport. Investigating the behaviours of Fig. 7 is a useful means of accomplishing this, since, in essence, R_{uw} quantifies how efficiently the available turbulence energy contributions combine to affect the turbulence momentum flux. This is a primary aim of the remaining analyses.

1. *Roughness and the logarithmic decay of R_{uw} with δ^+*

Using both low Reynolds number wind tunnel data and measurements from the nearly smooth neutrally stratified atmospheric surface layer, the analysis of Priyadarshana and Klewicki [39] revealed that R_{uw} decreases approximately logarithmically with Reynolds number. The smooth-wall results of Fig. 8 place this conclusion on much firmer ground by clearly demonstrating that the values of R_{uw} at z_I, as well as those of $\overline{u^2}$ and $\overline{w^2}$, follow logarithmic variations with δ^+ (recall that z_I is approximated differently for smooth- and rough-wall flows; comparisons between smooth- and rough-wall flows at matched $(z+\epsilon)/\delta$ are given in the following section). Additionally, the similarly plotted rough-wall data reveal that the purely δ^+ dependence apparent in the smooth-wall R_{uw} data is unambiguously modified by k_s^+ influences. The data of Fig. 8b indicate that the effect of decreasing k_s^+ is to increasingly attenuate the underlying growth in $\overline{u^2}(z_I)$ with δ^+ such that all of the rough-wall cases exhibit a slower rate of growth than for the smooth-wall. Conversely, the roughness effect on $\overline{w^2}(z_I)$ initially exhibits a steeper slope with increasing δ^+ than in smooth-wall flows, but with increasing k_s^+ the log-linear line becomes approximately parallel to that observed for the smooth-wall flow. From these observations, one is tempted to surmise that the dependence on δ^+ diminishes once k_s^+ crosses into the fully-rough regime. Such a conclusion is, however, deemed premature. This is because k_s^+ and δ^+ are not independently varied, and once in the fully rough regime the present data only cover a relatively small δ^+ range.

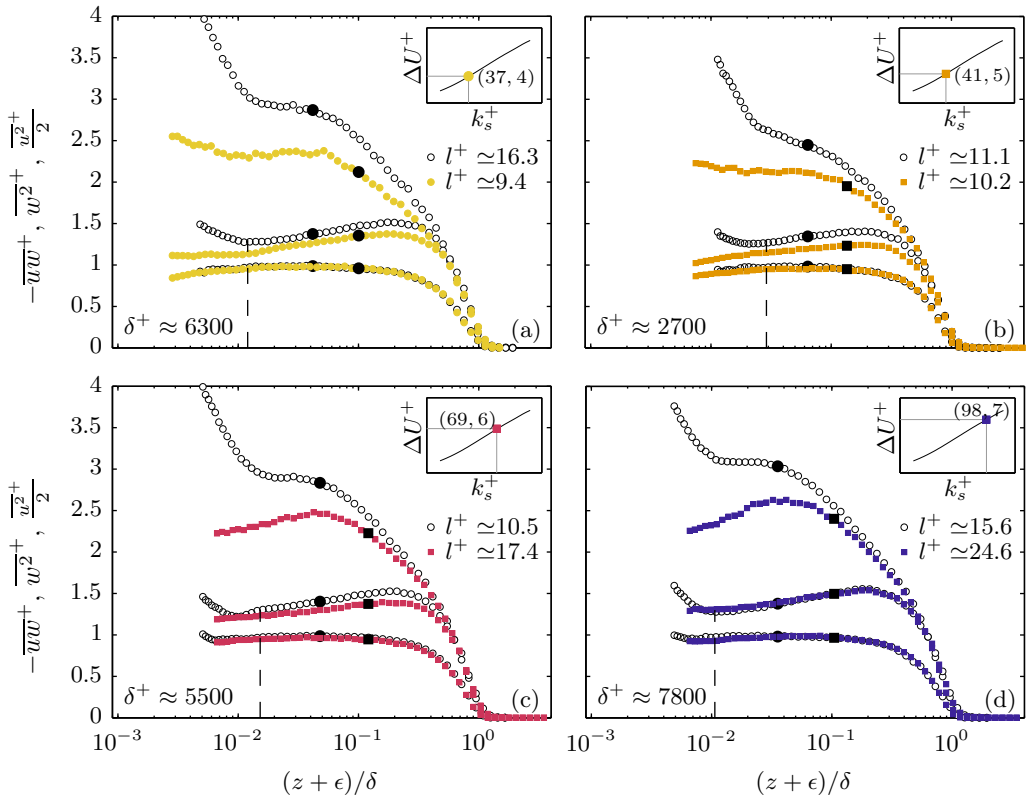

FIG. 9. Smooth-wall (open symbols) and rough-wall (filled,coloured symbols) streamwise velocity variance, wall-normal velocity variance, and Reynolds shear stress comparisons at approximately matched Reynolds numbers (shown in the top of each figure). The inset in each figure shows the k_s^+ and ΔU^+ values of the rough-wall data in that figure. The figures are ordered from low k_s^+ to high k_s^+. Black dashed lines show the location corresponding to $(z+\epsilon)^+ = 80$. The large black symbols show the onset of inertial dynamics, z_I, for each profile according to the formulation of Mehdi *et al.* [7]. Note that transitionally rough flows are characterized by $k_s^+ \lesssim 70$, while fully rough flows are characterized by $k_s^+ \gtrsim 70$.

Note, that the log-linear fits describing the k_s^+ effects are not theoretically motivated, and thus are included merely to aid in viewing the data trends. As $\delta^+ \to \infty$, the outer flow is anticipated (under outer similarity) to become k_s^+ invariant.

2. *Matched Reynolds number comparisons*

Extending the analysis of Squire *et al.* [4] for the streamwise variance, Fig. 9 compares smooth- and rough-wall $\overline{u^2}^+$, $\overline{w^2}^+$ and $-\overline{uw}^+$ profiles at four approximately matched δ^+. The sub-plots of Fig. 9 are ordered from top left to bottom right according to the magnitude of k_s^+. By examining flows at matched Reynolds number, k_s^+ trends are approximately isolated from those inherent to increasing δ^+. It is recognized, however, that the physical interpretation of these comparisons is complicated by the fact that δ^+ is nominally the ratio of largest and smallest scales of motion in the flow, and thus is indirectly influenced by k_s through the friction velocity. Similarly, although the value of k_s^+ connects to the generation of the wall-shear force (via viscous shear, pressure, or a combination of the two), there is ambiguity regarding its direct effect on the overall ratio of scales. As a result, δ^+ can only be assumed to approximately quantify similar dynamics between comparable δ^+ smooth- and rough-wall flows. Thus, the rationale for the comparisons of Fig. 9 is that they provide a nominal means of exploring k_s^+ influences, given an overall condition of scale separation as quantified by δ^+.

The $\overline{w^2}^+$ smooth-wall profiles exhibit a relatively abrupt upward near-wall trend. Morrill-Winter *et al.* [27] showed that this features correlates with physical wall-position, as opposed to inner-normalized distance. They hypothesized that the wall proximity produced a spatial confinement of the probe that artificially stimulated the cooling of its ×-array wires. In general, the existing literature provides little guidance regarding the characterization of such effects.

Morrill-Winter *et al.* [27] were, however, able to show that this effect seemed to be almost exclusively confined to $\overline{w^2}^+$, with no reliably attributable influence on U^+, $\overline{u^2}^+$ and $\overline{uw}^+$. Interestingly, for the rough-wall experiments this effect does not appear to be present. Accordingly, comparisons in Fig. 9 are only considered for $(z+\epsilon)^+ > 80$ (indicated by the black dashed lines in Fig. 9). Relative to objective comparisons, also note that, while the present measurements are well-resolved, they do not maintain the same spatial resolution between the rough- and smooth-wall cases. Relative to other experiments of this type, it is thus unclear how the present slight changes in l^+ might effect $\overline{w^2}^+$ or $\overline{uw}^+$. It is well-documented, however, that at any given wall normal location the length scales associated with $\overline{w^2}$ are smaller than those associated with $\overline{uw}$, e.g. [40], and thus the l^+ variations are expected to influence $\overline{w^2}^+$ to a greater degree – particularly near the wall. Recent studies have addressed this issue using DNS simulations, and reported that l^+ variations can either amplify or attenuate $\overline{w^2}^+$ – depending on the wall position. Amplification usually occurs for positions close to the wall, and under the condition of relatively poor spatial resolution, e.g. [41]. From the present data it is not possible to be precisely quantitative regarding spatial resolution effects. Given the present l^+ values, however, it seems safe to surmise that these effects are likely to be subtle. The l^+ values for each of the profiles are noted in Fig. 9.

For all the transitionally-rough flows in Fig. 9, differences between the smooth- and rough-wall $\overline{w^2}^+$ profiles extend well into the wake region. As discussed previously, this seems to be connected to a decreased amplitude of $\overline{w^2}^+$ at $(z+\epsilon)^+ \sim 80$ ($\overline{w^2}^+_{80}$); recall that $\overline{w^2}^+_{80}$ is essentially independent of δ^+ for smooth-wall flows [27]. The rate of increase of $\overline{w^2}^+$ beyond this point also seems to be the same for both smooth- and rough-wall flows. Interestingly, $(z+\epsilon)^+ \simeq 70$ is the outer limit of the near-wall cycle for smooth-wall flows [42]. It therefore seems likely that $\overline{w^2}^+_{80}$ is at least partially determined by the properties of this near-wall cycle, and accordingly, with the addition of roughness the flow properties in this region are altered. In particular, through the transitionally rough regime the near-wall cycle dynamics are increasingly perturbed, until this cycle is presumably no longer recognizable in the fully rough regime [6]. The variation of $\overline{w^2}^+_{80}$ depicted in Fig. 9a-d approximately coincides with the perturbation of the near-wall cycle, although the details regarding the profile behaviours and the specific modifications to the near-wall cycle are currently unknown. This observation is consistent with the findings presented in Fig. 6 relating to the peak in $\overline{w^2}^+$.

To within the uncertainty of the present experiments, the smooth- and rough-wall Reynolds stress profiles in figures 9a-d exhibit remarkable agreement. In particular, this agreement for a fixed δ^+ appears to hold across the outer domain regardless of k_s^+. As mentioned previously, the presence of a rough-wall causes the onset of inertial mean dynamics to move away from the wall for a fixed δ^+. Consistent with the formulations and discussion given by Mehdi *et al.* [7], the relative influences of the three length scales, ν/U_τ, k_s, and δ, describe the net behaviour of z_I. Thus, k_s^+ and δ^+ are connected to the peak location in $-\overline{uw}^+$, whereas this position only depends on δ^+ for smooth wall flows. Figure 9 qualifies this by showing that the rough-wall profiles decrease in magnitude relative to those in the smooth-wall flows in the region interior to z_I of the rough-wall. This is also demonstrated in Fig. 3. The observation is consistent with the generic observation that $z_m^+(k_s^+ \neq 0) > z_m^+(k_s^+ = 0)$. Also of interest, the $-\overline{uw}^+$ profiles are very similar between the two different boundary conditions, but for the transitionally rough profiles the ratio, $\overline{w^2}/|\overline{uw}|$, is larger for the smooth-wall flows, and is seemingly not a function of δ^+. The results of Fig. 9a-d and [4] indicate that this is similarly the case for $\overline{u^2}/|\overline{uw}|$. Such results suggest that, while the inner-normalized intensities of the relevant velocity components are attenuated at fixed δ^+ for the rough-wall profiles, their inner-normalized correlation is maintained when compared to the smooth-wall flow. The finding that $-\overline{uw}^+$ is similar in smooth- and rough-wall flows at fixed δ^+ is consistent with the mean momentum equation and the curvature of U^+ approaching the same value for $(z+\epsilon) \geq z_I$. It is interesting that with the apparent variations in the u and w velocity variances, the motions contributing to these two velocity components organize to preserve their correlation for $(z+\epsilon) \geq z_m$. Of course, the Reynolds shear stress, $\overline{uw}$, is representative of the net wallward flux of momentum, which is ultimately reflected by U_τ. Nonetheless, the observation motivates the spectral and quadrant analyses below.

3. *Reynolds shear stress co-spectra*

An indication of the correlating scales of motion that lead to the Reynolds shear stress profiles in Fig. 9 is gained through consideration of the inner-normalised co-spectral density of the streamwise and wall-normal velocity fluctuations (from here on just called the cospectra). Figure 10 presents a comparison of smooth- and rough-wall cospectra throughout the inertial subdomain for the Reynolds numbers considered in Fig. 9. Wavelengths were approximated using Taylor's [43] hypothesis and the local mean velocity. While this is a common approach to estimate a spatial derivative from a time series, relative to smooth-wall flows there is less justification for the application of Taylor's hypothesis in rough-wall flows since the turbulence intensities as a proportion of the local mean can be significantly

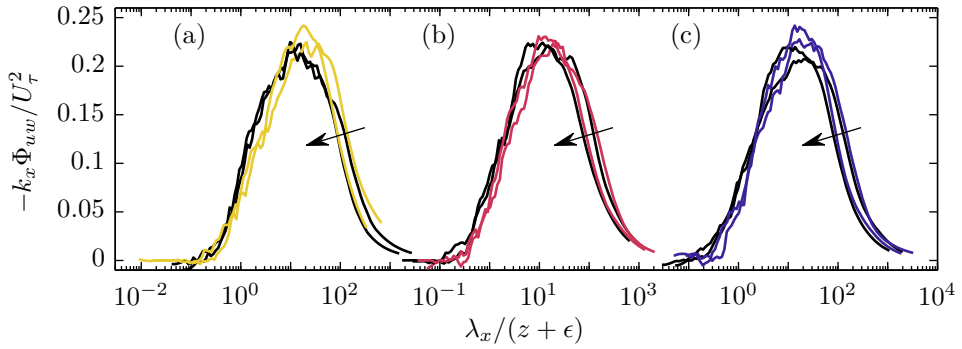

FIG. 10. Comparison of smooth- (black lines) and rough-wall (colored lines) cospectra of streamwise and wall-normal velocity fluctuations at approximately matched δ^+. Rough-wall profiles are colored as indicated in table I. Cospectra are shown at $(z+\epsilon) = z_I$ and $(z+\epsilon) = 0.19\delta$ for each matched δ^+ comparions, with the black arrow indicating increasing $(z+\epsilon)$. In (a), (b) and (c), the same comparions as in figure 9(a), (c) and (d), respectively, are shown ($\delta^+ \approx 6300, 5500, 7800$).

larger. Recently, Squire *et al.* [44] demonstrated that the application of Taylor's hypothesis in rough-wall flows can produce erroneous estimates of spectra involving the wall-normal velocity component. We therefore emphasize that prescribing the mean velocity to be the advection velocity for each scale over both wall conditions can, at best, provide only an approximate representation of wavelength.

According to prevalent theories, once on the inertial domain, the momentum transporting motions exhibit *distance from the wall* scaling across a self-similar hierarchy of layers (for example, the L_β hierarchy—see [45] and [7]—and the attached-eddy hypothesis—see [46]). In the smooth-wall case, the relationship from one member of the hierarchy to the next is solely a function of Reynolds number. In the rough-wall case, the expectation is that the scaling behaviour from one hierarchy to the next is, in general, a function of roughness and Reynolds number. Since the influence of roughness on the hierarchy is not explicitly known, a continuous description of the layer transitions is beyond our current understanding. We do, however, know that for both smooth- and rough-wall flows the inertial layer begins near z_I and ends near $(z+\epsilon)/\delta = 0.19$ (see [4]). Additionally, Priyadarshana and Klewicki [39] used a filter based analysis to estimate the predominant frequency (wavelength) contributions to the uw signal. Somewhat contrary to accepted notions, they found that even at very high Reynolds numbers these contributions are associated with motions that are intermediate in size relative to the inner and outer scales. Similarly, Ebner *et al.* [8] observed that normalizations using z_I are effective at bringing statistical profiles from disparate roughness surfaces into nominal agreement. With these considerations in mind, Fig. 10 presents cospectra at $(z+\epsilon) = z_I$ and $(z+\epsilon) = 0.19\delta$ for each matched δ^+ comparison. (Recall from §II that z_I is defined differently for the smooth and rough walls; these definitions do not coincide in either inner or outer scaling, but instead identify the same mean dynamical condition). To emphasize the *distance from the wall* scaling stipulated by the theories just mentioned, the wavelength in Fig. 10 is normalized by its respective wall-normal location, $(z+\epsilon)$.

Given the previously mentioned uncertainties associated with the application of Taylor's hypothesis, the cospectral comparisons in Fig. 10 show inertial region invariance between smooth- and rough-wall flows across all values of k_s^+ examined. The statistical comparisons in Fig. 9 indicate clear differences in the outer region between the smooth and rough wall streamwise and wall-normal intensities at low k_s^+. Yet the apparent invariance of the curves in Fig. 10 suggests that, despite the differences in the energy content of the individual velocity component constiuents of the Reynolds shear stress, the strength and scales of the velocity correlation in the inertial region is somehow maintained between the smooth- and rough-wall flows. Fully elucidating the above observations requires further investigation of the correlating scales of motion that lead to the apparent differences between the smooth and rough wall flow behaviours exhibited in Figs. 7 and 9. On the other hand, Fig. 10 clarifies that, consistent with wall scaling, these differences do not arise from any significant modifications to the interacting scales of the u and w motions. Insights into the observed differences are, however, further enabled through quadrant analysis of the Reynolds shear stress correlation.

4. Quadrant analysis

Wallace *et al.* [47] introduced the conditional analysis of the Reynolds shear stress contributions on the basis of the four possible signed combinations of u and w, referred to as Q1, Q2, Q3 and Q4 events. Quadrant analysis provides

a useful way to expose the nature of the u and w combinations that contribute to $\overline{uw}$. Such analysis was particularly relevant in explaining the behaviours observed in the flow visualisations of Grass [48]. These revealed that, above regular gravel-type roughness, violent ejection (Q2) events span much of the wall layer, while the sweep motions (Q4) are confined to the region close to the wall. In the subsequent literature, there are rough-wall studies that report an increase [17, 49, 50], a decrease [14, 51], and a negligible change [15, 52] in Q2 activity relative to smooth-wall flow. Similar uncertainty in the effect of roughness is reported relative to Q4 events. Here we present uniformly well-resolved data that enable the conditional structure of the Reynolds shear stress to be examined over a unique range of parameters. This is particularly pertinent in light of Fig. 9 showing that at low k_s^+ the present rough-wall attenuates the inner-normalised streamwise and wall-normal velocity fluctuations relative to the smooth-wall flow, even though the smooth- and rough-wall $\overline{uw}^+$ profiles show very good agreement.

A quadrant decomposition using the hyperbolic hole approach of Lu and Willmarth [53] is performed. Here the percentage contribution to $\overline{uw}$ from a given quadrant, P_Q, is given by

$$P_Q = Prob_Q(H) = \lim_{T\to\infty} \frac{1}{T\overline{uw}} \int_0^T uw(t) I_Q(t,H) dt. \tag{4}$$

Here, t represents time, and I_Q is an indicator function:

$$I_Q = \begin{cases} 1, & \text{when } |uw|_Q \geq H\sqrt{\overline{u^2}}\sqrt{\overline{w^2}} \\ 0, & \text{otherwise.} \end{cases} \tag{5}$$

The time fraction, T_Q, spent in a particular quadrant is computed from

$$T_Q(H) = \frac{1}{T} \int_0^T I_Q(t,H) dt. \tag{6}$$

The hyperbolic hole size, H, sets the magnitude of the threshold for events to be included in the conditional sample with $H = 0$ corresponding to including all events within a particular quadrant. Figure 11 shows the results of the quadrant analysis for $H = 0$ (first row) and $H = 1$ (second row). In Figs. 11(a) and (c), each of (i), (ii) and (iii) compares the percentage contribution from Q2 and Q4 events to the total Reynolds shear stress above smooth- and rough-wall flows at the three approximately matched δ^+. The same comparisons as were presented in Fig. 9(a), (c) and (d) are presented here; recall that the rough-wall profiles are for $k_s^+ = 37$, 68 and 97, respectively, but are all at $\delta^+ = 6600 \pm 1200$.

Figure 11(a) shows that the present rough-wall modifies the u and w structure relative to the smooth-wall flow. Across all three matched Reynolds number comparisons, the rough-wall appears to generate a decrease in Q2 activity, while the percentage contribution from Q4 is less affected – especially in the outer region. The Q2 results indicate a reduction in the strength and/or frequency of ejection events. In Fig. 11(b), the time fractions, T_2 and T_4, show good agreement between the smooth- and rough-wall for all three comparisons. This suggests that the smooth/rough differences in Fig. 11(a) result from modified strength, not frequency, of the Q2 events. This modification also requires redistributions of the event amplitude probabilities associated with Q1 and Q3 events, since the total percentage from all four quadrants must always sum to 100%.

As demonstrated in Fig. 11(b), neither P_2 or P_4 show discernible differences between the smooth-wall cases across the present range of friction Reynolds numbers. This supports the notion that (i), (ii) and (iii) are sufficiently close in δ^+ to approximately isolate trends with k_s^+. Like for the smooth-wall flows, the distributions of P_2 from the rough-wall experiments appear to be relatively unaffected by roughness Reynolds number. Conversely, P_4 increases across the entire boundary layer as the flow progresses towards the fully rough condition. For $H = 1$ (second row of Fig. 11), similar trends to those described above are observed, but there are more significant differences between the smooth- and rough-wall Q4 contributions – at least at high k_s^+. Note that the $H = 1$ threshold isolates only large excursions. Specifically, its use results in the consideration of less than 10% of the uw time-series at all wall-normal locations.

T_{2+4} quantifies the time fraction that uw is producing a wallward flux of momentum. Analyses revealing self-similar structure admitted by the mean momentum equation suggest that this fraction asymptotically approaches a constant value, ϕ_c^{-1} [54]. These analyses also indicate that ϕ_c^2 is equal to the inverse of the leading coefficient in the log law for the mean profile, i.e., one over the von Kármán constant. Furthermore, under a natural extension to *distance from the wall* scaling one arrives at the prediction that on the inertial domain $\phi_c^{-1} = \Phi^{-1} = 2/(1+\sqrt{5}) \simeq 0.618$, the inverse of the golden ratio. Relative to the present interest in outer-similarity, it is thus instructive to compare the differing δ^+ behaviours of T_{2+4} for the present variations in k_s^+.

Figure 12 presents profiles of T_{2+4} versus $(z+\epsilon)/z_I$. As is apparent, the smooth wall profiles on this graph attain a convincing plateau on the inertial domain, and the width of this plateau grows with increasing δ^+. Also with

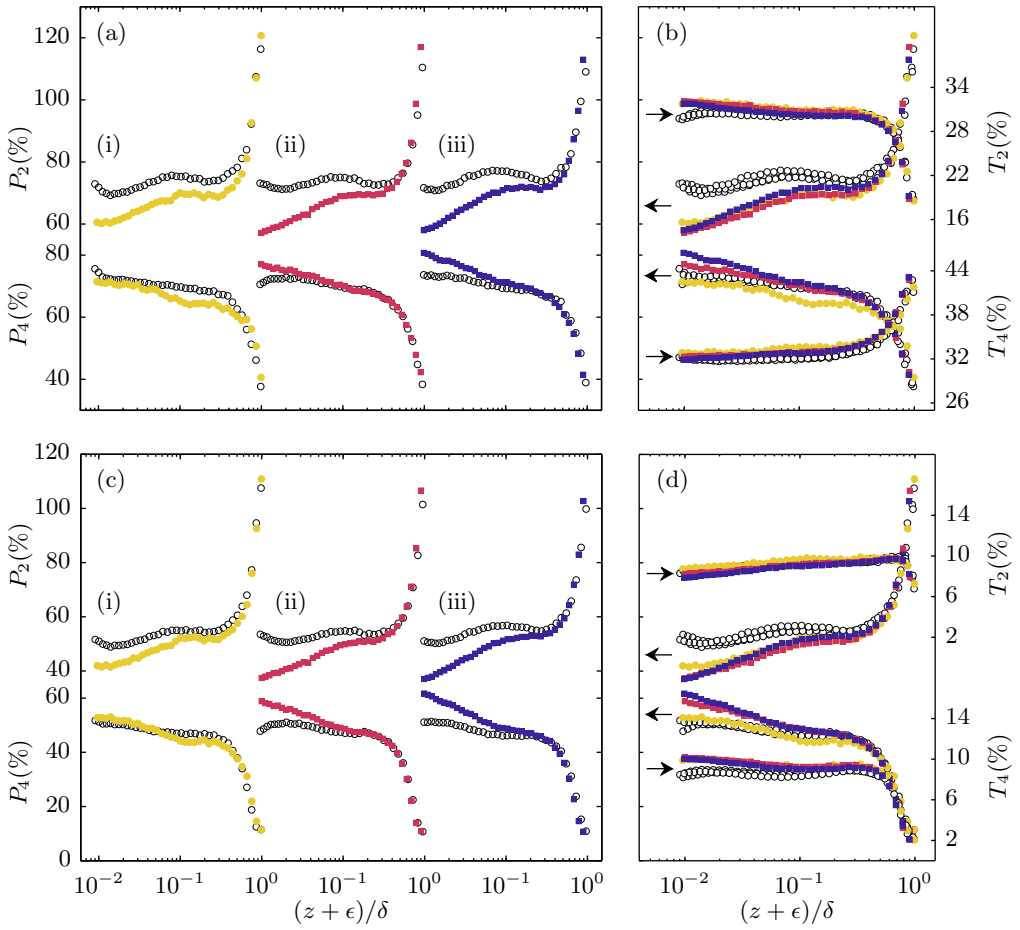

FIG. 11. Quadrant decomposition of the Reynolds shear stress into percentage contributions from Q2 and Q4 events. The results in the first row ((a) and (b)) are computed using $H = 0$, while those in the second row ((c) and (d)) use $H = 1$. In (a) and (c), each of (i), (ii), (iii) compares the percentage contribution from Q2 and Q4 above a smooth-wall (open symbols) and rough-wall (filled, coloured symbols) flow at matched friction Reynolds number ($Re_\tau \approx 6300$, 5500 and 7800 in (i), (ii) and (iii), respectively). The roughness Reynolds number of the rough-wall data in these comparisons is $k_s^+ = 37$, 68 and 97, respectively. Note that transitionally rough flows are characterized by $k_s^+ \lesssim 70$, while fully rough flows are characterized by $k_s^+ \gtrsim 70$. In (b) and (d), all three matched Reynolds number comparisons are plotted to demonstrate trends with k_s^+. Here, the percentage contributions from each event (P_2 and P_4), and the time fractions associated with each event (T_2 and T_4, respectively) are shown, with the black arrows indicating which data corresponds to which axis.

increasing δ^+ (and over the given δ^+ range), the plateau value appears to approach something near to that surmised by Klewicki *et al.* [54]. The rough-wall data on the plot exhibit a similar trend with δ^+. For the given δ^+ range, however, T_{2+4} is consistently larger than the smooth-wall flow at comparable δ^+. Presuming that an asymptotic value of T_{2+4} exists, then relative to inertial domain momentum transport this value should be reflective of the condition of outer similarity. This leads to the intriguing observation that the addition of the present roughness delays the approach to this asymptotic state. The subject behaviour is made clearer in Fig. 13, which plots the value of T_{2+4} averaged over the inertial domain versus δ^+. From Fig. 12, it also seems clear that the apparent differences between the smooth- and rough-wall T_{2+4} profiles near the wall reflect the direct amplifying effect that roughness has on turbulent momentum transport in this region.

Lastly, we use the result of Fig. 13 to make a broader cautionary observation regarding the notion of scale separation in rough-wall flows. In this figure, the behaviour of the rough-wall data seems to suggest that the approach to the asymptotic state is a slower function of δ^+ in the rough-wall flows. Insight into this issue is gained by first noting that δ^+ is the ratio of length scales, δ to ν/U_τ. With the addition of roughness, however, additional length scales are imposed upon, and nonlinearly modify, the scales ranging from $\mathcal{O}(\nu/U_\tau)$ to $\mathcal{O}(\delta)$. On average, roughness modifies (generally increases) the position where the flow transitions to inertial mean dynamics. Herein, the characteristic

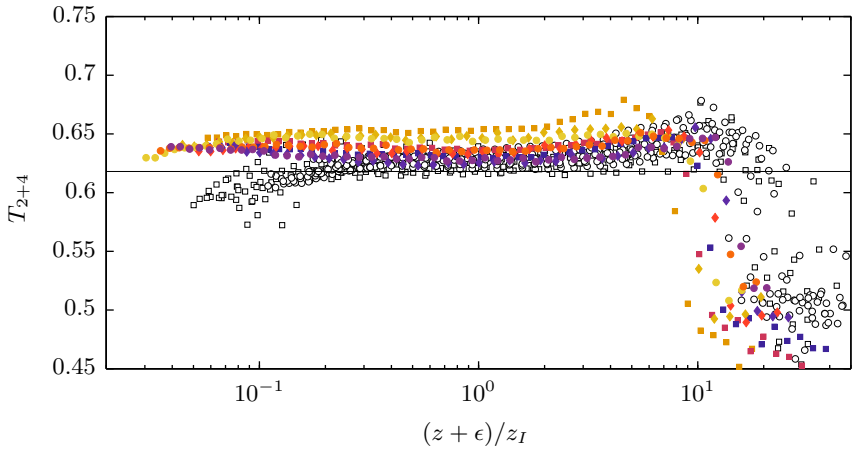

FIG. 12. Time fraction that uv is negative versus wall-normal distance normalized by the onset of inertial dynamics. The rough wall symbols are tabulated in I. The open symbols are all the smooth-wall data of Morrill-Winter *et al.* [27] (refer to publication for boundary layer parameters): ○ represent data acquired in the Melbourne Wind Tunnel, where □ signify data taken in the FPF. The black horizontal lines represent $\overline{T}_{2+4} = 0.618$.

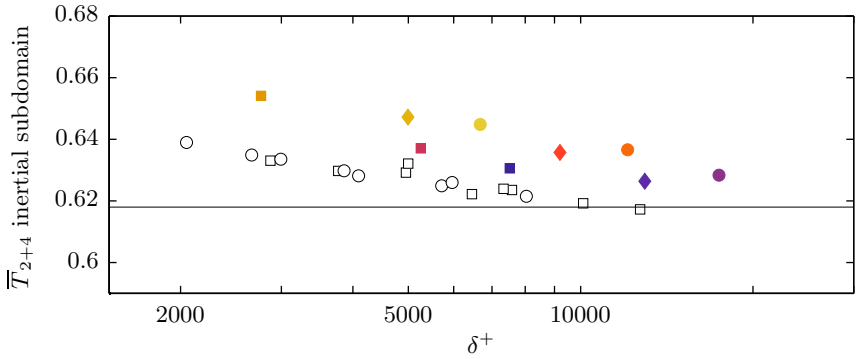

FIG. 13. The average time fraction that uw is negative in the inertial domain versus Reynolds number. The rough wall symbols are tabulated in I. The open symbols are all the smooth-wall data of Morrill-Winter *et al.* [27] (refer to publication for boundary layer parameters): ○ represent data acquired in the Melbourne Wind Tunnel, where □ signify data taken in the FPF. The black horizontal lines represent $\overline{T}_{2+4} = 0.618$.

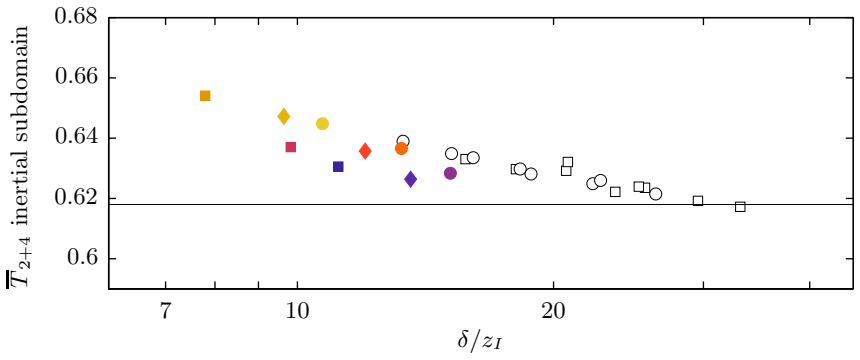

FIG. 14. The average time fraction that uw is negative in the inertial domain versus Reynolds number normalized by the onset of inertial dynamics. The rough wall symbols are tabulated in I. The open symbols are all the smooth-wall data of Morrill-Winter *et al.* [27] (refer to publication for boundary layer parameters): ○ represent data acquired in the Melbourne Wind Tunnel, where □ signify data taken in the FPF. The black horizontal lines represent $\overline{T}_{2+4} = 0.618$.

length scale of the largest motion affected by a leading order viscous force is estimated by z_I. Accordingly, a measure of the scale separation between the characteristic inertial scale and this scale is δ/z_I. Figure 14 re-plots the data of Fig. 13 according to this new measure of scale separation. If the asymptote suggested on Fig. 14 is valid, then the smooth-wall data suggest that a value of $\delta/z_I \gtrsim 20$ is required to attain this indicator of self-similar structure on the inertial domain. As is apparent, by this measure the degree of scale separation is considerably smaller than this in the present rough-wall flows.

IV. CONCLUSIONS

Measurements associated with the turbulent stresses, $\overline{u^2}$, $\overline{w^2}$ and $\overline{uw}$, were acquired above the same sandpaper surface that Squire *et al.* [4] used to study the effects of roughness and Reynolds number on U and $\overline{u^2}$. The present measurements were acquired using a multi-element hot-wire sensing array, and covered a distinctively broad range of Reynolds number and equivalent sand grain roughness $2,800 \lesssim \delta^+ \lesssim 17,400$ and $37 \lesssim k_s^+ \lesssim 98$, respectively. Numerous comparisons are made between these measurements, and those acquired in smooth-wall boundary layers by Morrill-Winter *et al.* [27] over a comparable δ^+ range. To the authors' knowledge, such comparisons are also distinctive in that they involved data from an identical sensor, and these sensors maintained very good spatial resolution over the entire range of parameters. Important features of the present experiments are the spatially well-resolved nature of the turbulence measurements, and the direct, and quasi-direct measurement, of the wall-shear stress. Notably, all of the present profiles show self-consistent trends with δ^+ and k_s^+.

The mean momentum equation is the same for both smooth- and rough-walled turbulent boundary layers. Also, the wall-normal gradient of the mean velocity beyond the start of the inertial domain is not influenced by the surface condition. From this, inner-normalized Reynolds stress profiles at a fixed δ^+ are not expected to differ in the inertial domain. These features were shown to hold for the present data. Using the formulation of Mehdi *et al.* [7], the onset of the inertial domain, z_I, was estimated. When the wall position was normalized by z_I, both the smooth- and rough-wall Reynolds stress peaks seemingly align, thus corroborating the empirical curve-fits of Mehdi *et al.* [7] for the given k_s/z_I regime. For all of the present measurements, the peak magnitude in $-\overline{uw}^+ \simeq 1$ and never exceeded unity. This further reinforced the validity of the approach introduced by Squire *et al.* [4] to determine U_τ at streamwise locations where drag balance data was not directly available.

When compared to smooth-wall profiles at approximately matched δ^+, the present wall-normal velocity variance profiles in the transitionally rough regime exhibit a reduction in magnitude over the domain $(z+\epsilon)^+ \gtrsim 80$. Such behaviour is consistent with the gradual roughness-induced perturbation of the near-wall cycle. In particular, the mechanisms of this cycle are expected to diminish as the pressure contribution to the surface drag (due to separated flow around the roughness elements) becomes increasingly large in comparison to the viscous contribution; i.e., as the flow transitions to the fully-rough regime. Akin to smooth-wall flow behaviours, for increasing positions beyond $(z+\epsilon)^+ \simeq 80$ the present rough-wall profiles exhibit a self-consistent upward trajectory out to $(z+\epsilon)/\delta \simeq 0.19$. Furthermore, combining this behaviour with $\overline{w^2}^+_{80} = f(k_s^+)$ explains the reduced peak magnitude of $\overline{w^2}^+$ at fixed δ^+ for $k_s^+ < 70$. When the maxima of $\overline{w^2}^+$ are plotted versus δ^+, the fully-rough profiles show good agreement with the smooth-wall data, whereas, the transitionally rough data are of lower amplitude. The rate of increase with respect to δ^+, however, appears to be an inverse function of k_s^+. None of the present transitionally rough-wall data support the validity of outer similarity over the present δ^+ range. Based upon the previous analyses of Kunkel and Marusic [38], these results are interpreted to suggest that the present δ^+ are insufficient to approximately reflect Townsend's hypothesis for this statistic in this roughness regime. This result stands in contrast to previous findings pertaining to this statistic.

The rough-wall profiles of Reynolds stress correlation coefficient, R_{uw}, exhibit elevated values relative to their matched Reynolds number smooth-wall profiles. Like the smooth-wall profiles, however, the rough-wall R_{uw} exhibit an approximately logarithmic decrease with δ^+. The rate of logarithmic decrement with δ^+ varies, however, with k_s^+, thus highlighting the combined roughness and Reynolds number influences on the turbulent flux of momentum. Because the $\overline{uw}^+$ profiles exhibit only subtle changes between the smooth- and rough-wall flows, the variations in R_{uw} are predominantly connected to the individual variations in $\overline{u^2}^+$ and $\overline{w^2}^+$. Here, the present results suggest that, increasing k_s^+ flattens the logarithmic increase in $\overline{u^2}^+(z_I)$ (relative to the smooth-wall case). The same trend is also observed for $\overline{w^2}^+(z_I)$, but in this case the slope does not decrease below that of the smooth wall.

The present cospectra of u and w suggest that the inertial layer contributions to $\overline{uw}$ involve the same normalized spectral content (range and amplitudes) regardless of k_s^+. The distance from the wall normalization required to realize this condition is consistent with the existence of a hierarchical structure to inertial layer turbulence, essentially independent of the value of k_s^+. The physical mechanisms that yield the invariant cospectra, despite variations in the spectral content of both u and w, are presently unknown.

Normalized contributions to the Reynolds stress from the second (Q2) and fourth (Q4) quadrants were evaluated at an approximately fixed δ^+ for three different roughness-Reynolds number combinations. For all the k_s^+ values, the Q2 contributions decreased in activity, especially near the wall, while the Q4 contributions appeared less affected. This result did not substantially change when the hyperbolic hole size, H, was increased from 0 to 1. Q4 events, however, were shown to increase in magnitude over the entire boundary layer with increasing k_s^+. The present quadrant analyses indicate that, while the inner-normalized Reynolds stress shows similarity over the smooth- and rough-surface, the relevant probabilities underlying the subtly varying $\overline{uw}$ structure is a complicated function of k_s^+ and δ^+ for the parameter ranges investigated.

Finally, the rescaling presented in Fig. 14 raises questions about the validity of matched δ^+ comparisons between smooth- and rough-wall flows. The results in Fig. 14 suggest that the ratio δ/z_I may provide an alternative view of the true scale separation (and hence an alternative appropriate Reynolds number for these flows). The present data are suggestive in this regard, but a wider range of matched δ/z_I smooth- and rough-wall data are required before informative conclusions can be drawn.

ACKNOWLEDGMENTS

The authors wish to thank the Australian Research Council for the financial support of this research. MPS would like to thank the U.S. Office of Naval Research for supporting his sabbatical visit to the University of Melbourne.

[1] M. R. Raupach, R. A. Antonia, and S. Rajagopalan, "Rough-wall turbulent boundary layers," Appl. Mech. Rev. **44**, 1–25 (1991).
[2] F. H. Clauser, "Turbulent boundary layers in adverse pressure gradients," J. Aeronaut. Sci. **21**, 91–108 (1954).
[3] F. R. Hama, *Boundary-layer characteristics for smooth and rough surfaces* (Trans SNAME, 1954) pp. 333–351.
[4] D. T. Squire, C. Morrill-Winter, N. Hutchins, M. P. Schultz, J. C. Klewicki, and I. Marusic, "Comparison of turbulent boundary layers over smooth and rough surfaces up to high Reynolds numbers," J. Fluid Mech. **795**, 210–240 (2016).
[5] A. E. Perry, W. H. Schofield, and P. N. Joubert, "Rough wall turbulent boundary layers," J. Fluid Mech. **37**, 383–413 (1969).
[6] J. Jiménez, "Turbulent flows over rough walls," Annu. Rev. Fluid Mech. **36**, 173–196 (2004).
[7] F. Mehdi, J. C. Klewicki, and C. M. White, "Mean force structure and its scaling in rough-wall turbulent boundary layers," J. Fluid Mech. **731**, 682–712 (2013).
[8] R. L. Ebner, Mehdi F., and J.C. Klewicki, "Shared dynamical features of smooth- and rough-wall boundary-layer turbulence," J. Fluid Mech. **792**, 435–469 (2016).
[9] J. Nikuradse, "Laws of flow in rough pipes," NASA Tech. Memo. (1933).
[10] A. A. Townsend, *The Structure of Turbulent Shear Flow* (Cambridge University Press, 1976).
[11] A. E. Perry and C. J. Abell, "Asymptotic similarity of turbulence structures in smooth-and rough-walled pipes," J. Fluid Mech. **79**, 785–799 (1977).
[12] M. R. Raupach, "Conditional statistics of Reynolds stress in rough-wall and smooth-wall turbulent boundary layers," J. Fluid Mech. **108**, 363–382 (1981).
[13] M. Acharya, J. Bornstein, and M. P. Escudier, "Turbulent boundary layers on rough surfaces," Exp. Fluids **4**, 33–47 (1986).
[14] P.-Å Krogstad, H. I. Andersson, O. M. Bakken, and A. Ashrafian, "An experimental and numerical study of channel flow with rough walls," J. Fluid Mech. **530**, 327–352 (2005).
[15] K. A. Flack, M. P. Schultz, and T. A. Shapiro, "Experimental support for Townsend's Reynolds number similarity hypothesis on rough walls," Phys. Fluids **17**, 035102 (2005).
[16] R. J. Volino, M. P. Schultz, and K. A. Flack, "Turbulence structure in rough-and smooth-wall boundary layers," J. Fluid Mech. **592**, 263–293 (2007).
[17] P.-Å Krogstad, R. A. Antonia, and L. W. B. Browne, "Comparison between rough-and smooth-wall turbulent boundary layers," J. Fluid Mech. **245**, 599–617 (1992).
[18] M. F. Tachie, D. J. Bergstrom, and R. Balachandar, "Rough wall turbulent boundary layers in shallow open channel flow," J. Fluids Engng **122**, 533–541 (2000).
[19] L. Keirsbulck, L. Labraga, A. Mazouz, and C. Tournier, "Surface roughness effects on turbulent boundary layer structures," J. Fluids Engng **124**, 127–135 (2002).
[20] S. Leonardi, P. Orlandi, R. J. Smalley, L. Djenidi, and R. A. Antonia, "Direct numerical simulations of turbulent channel flow with transverse square bars on one wall," J. Fluid Mech. **491**, 229–238 (2003).
[21] K. Bhaganagar, J. Kim, and G. Coleman, "Effect of roughness on wall-bounded turbulence," Flow Turbul. Combust. **72**, 463–492 (2004).

[22] S.-H. Lee and H. J. Sung, "Direct numerical simulation of the turbulent boundary layer over a rod-roughened wall," J. Fluid Mech. **584**, 125–146 (2007).

[23] V. Efros and P.-Å Krogstad, "Development of a turbulent boundary layer after a step from smooth to rough surface," Exp. Fluids **51**, 1563–1575 (2011).

[24] T. Meyers, J. B. Forest, and W. J. Devenport, "The wall-pressure spectrum of high-Reynolds-number turbulent boundary layer flows over rough surfaces," J. Fluid Mech. **768**, 261–293 (2015).

[25] D. T. Squire, C. Morrill-Winter, N. Hutchins, I. Marusic, M. P. Schultz, and J. C. Klewicki, "Smooth-and rough-wall boundary layer structure from high spatial range particle image velocimetry," Phys. Rev. Fluids **1**, 064402 (2016).

[26] D. T. Squire, W. J. Baars, N. Hutchins, and I. Marusic, "Inner–outer interactions in rough-wall turbulence," J. Turbul. **17**, 1159–1178 (2016).

[27] C. Morrill-Winter, J. Klewicki, R. Baidya, and I. Marusic, "Temporally optimized spanwise vorticity sensor measurements in turbulent boundary layers," Exp. Fluids **56**, 1–14 (2015).

[28] T. B. Nickels, I. Marusic, S. Hafez, and M. S. Chong, "Evidence of the k_1^{-1} law in a high-Reynolds-number turbulent boundary layer," Phys. Rev. Let. **95**, 074501 (2005).

[29] T. B. Nickels, I. Marusic, S. Hafez, N. Hutchins, and M. S. Chong, "Some predictions of the attached eddy model for a high Reynolds number boundary layer," Phil. Trans. Roy. Soc. A **365**, 807–822 (2007).

[30] J. F. Foss and R. C. Haw, "Transverse vorticity measurements using a compact array of four sensors," Symp. on Thermal Anemometry (ASME FED, 1990).

[31] W. J. Baars, D. T. Squire, K. M. Talluru, M. R. Abbassi, N. Hutchins, and I. Marusic, "Wall-drag measurements of smooth- and rough-wall turbulent boundary layers using a floating element," Exp. Fluids. **57**, 1–16 (2016).

[32] I. Marusic, J. Monty, M. Hultmark, and A. Smits, "On the logarithmic region in wall turbulence," J. Fluid Mech. **716, R3** (2013).

[33] K. A. Chauhan, P. A. Monkewitz, and H. M. Nagib, "Criteria for assessing experiments in zero pressure gradient boundary layers," Fluid Dyn. Res. **41**, 021404 (2009).

[34] J. A. Sillero, J. Jiménez, and R. D. Moser, "One-point statistics for turbulent wall-bounded flows at Reynolds numbers up to $\delta^+ \approx 2000$," Phys. Fluids **25**, 105102 (2013).

[35] M. P. Schultz and K. A. Flack, "The rough-wall turbulent boundary layer from the hydraulically smooth to the fully rough regime," J. Fluid Mech. **580**, 381–405 (2007).

[36] T. Wei, P. Fife, J. Klewicki, and P. McMurtry, "Properties of the mean momentum balance in turbulent boundary layer, pipe and channel flows," J. Fluid Mech. **522**, 303 – 327 (2005).

[37] H. Tennekes and J. Lumley, *A First Course in Turbulence* (The MIT Press, 1994).

[38] G. J. Kunkel and I. Marusic, "Study of the near-wall-turbulent region of the high-Reynolds-number boundary layer using an atmospheric flow," J. Fluid Mech. **548**, 375–402 (2006).

[39] P. J. A. Priyadarshana and J. C. Klewicki, "Study of the motions contributing to the Reynolds stress in high and low Reynolds number turbulent boundary layers," Phys. Fluids **16**, 4586 – 4600 (2004).

[40] T. Wei and W. W. Willmarth, "Reynolds number effects on the structure of turbulent channel flow," J. Fluid Mech. **204**, 57 – 95 (1989).

[41] J. Philip, R. Baidya, N. Hutchins, J. P. Monty, and I. Marusic, "Spatial averaging of streamwise and spanwise velocity measurements in wall-bounded turbulence using ⋁-and ×-probes," Meas. Sci. Tech. **24**, 115302 (2013).

[42] J. Jiménez and A. Pinelli, "The autonomous cycle of near-wall turbulence," J. Fluid Mech. **389**, 335–359 (1999).

[43] G. I. Taylor, "The spectrum of turbulence," in *Proc. R. Soc. Lond. A*, Vol. 164 (The Royal Society, 1938) pp. 476–490.

[44] D. T. Squire, N. Hutchins, C. Morrill-Winter, M. P. Schultz, J. C. Klewicki, and I. Marusic, "Applicability of Taylor's hypothesis in rough-and smooth-wall boundary layers," J. Fluid Mech. **812**, 398–417 (2017).

[45] J. C. Klewicki, "Self-similar mean dynamics in turbulent wall-flows," J. Fluid Mech. **718**, 596–621 (2013).

[46] A. E. Perry and I. Marusic, "A wall-wake model for the turbulence structure of boundary layers. Part 1. Extension of the attached eddy hypothesis," J. Fluid Mech. **298**, 361–388 (1995).

[47] J. Wallace, H. Eckelmann, and R. Brodkey, "The wall region in turbulent shear flow," J. Fluid Mech. **54**, 39–48 (1972).

[48] A. J. Grass, "Structural features of turbulent flow over smooth and rough boundaries," J. Fluid Mech. **50**, 233–255 (1971).

[49] M. P. Schultz and K. A. Flack, "Outer layer similarity in fully rough turbulent boundary layers," Exp. Fluids **38**, 328–340 (2005).

[50] S. Leonardi, *Turbulent channel flow with roughness: direct numerical simulations*, Ph.D. thesis, Universita di Roma (2002).

[51] P.-Å Krogstad and R. A. Antonia, "Surface roughness effects in turbulent boundary layers," Exp. Fluids **27**, 450–460 (1999).

[52] Y. Wu and K. T. Christensen, "Outer-layer similarity in the presence of a practical rough-wall topography," Phys. Fluids **19**, 85108–85108 (2007).

[53] S. S. Lu and W. W. Willmarth, "Measurements of the structure of the Reynolds stress in a turbulent boundary layer," J. Fluid Mech. **60**, 481–511 (1973).

[54] J. C. Klewicki, J. Philip, I. Marusic, K. Chauhan, and C. Morrill-Winter, "Self-similarity in the inertial region of wall turbulence," Phys. Rev. E **90**, 063015 (2014).